# Self-Assembled Monolayers of 2-Adamantanethiol on Au{111}: Control of Structure and Displacement†

**Moonhee Kim,‡ J. Nathan Hohman,‡ Elizabeth I. Morin,‡ Thomas A. Daniel,§ and Paul S. Weiss*,‡**

*Departments of Chemistry and Physics, 104 Davey Laboratory, and The Materials Research Institute, 102 Materials Research Building, The Pennsylvania State University, University Park, Pennsylvania 16802*

*Received: November 14, 2008; Revised Manuscript Received: February 6, 2009*

We have investigated the formation of 2-adamantanethiolate self-assembled monolayers on Au{111} and their displacement by *n*-dodecanethiol, using scanning tunneling microscopy, X-ray photoelectron spectroscopy, and infrared reflection absorption spectroscopy. Well-ordered 2-adamantanethiolate monolayers undergo rapid and significant molecular exchange upon exposure to *n*-dodecanethiol solutions, but their structures and intermolecular interactions template the growth of *n*-dodecanethiolate domains. Annealing 2-adamantanethiolate monolayers at 78 °C decreases the density of vacancy islands, while increasing the overall order and the average domain sizes in the films. This results in slower displacement by *n*-dodecanethiol molecules, as compared to unannealed monolayers. The secondary sulfur position on the adamantyl cage influences the lattice structure and exchange of 2-adamantanethiolate monolayers by alkanethiols.

## 1. Introduction

Alkanethiolate self-assembled monolayers (SAMs) on Au{111} form well-defined crystalline structures due to the spontaneous formation of strong gold−sulfur bonds and attractive van der Waals forces between adjacent alkyl chains.[1,2] However, characteristic domain boundaries and defects generated during assembly[3−6] limit their applicability for patterning and device fabrication.[6−8]

One solution for improving control over patterning in SAMs is to design molecules with tailored intermolecular interactions that impart tunability to surface properties.[9−15] For instance, self-assembly of amide-containing alkanethiols results in highly stable films due to strong hydrogen bonding interactions between buried amide functional groups.[16,17] In contrast, adamantanethiols with their rigid 10-carbon adamantane cage (Scheme 1)[18] produce SAMs with larger intermolecular distances and thus smaller intermolecular interaction strengths, as compared to *n*-alkanethiols. Thiol-based adamantane[19−21] and polymantane[22−24] SAMs on Au{111} have been prepared with a variety of assemblies on gold surfaces by altering the number and position of thiol functionalities on the diamondoid cage. Recent scanning tunneling microscopy (STM) studies on 1-adamatanethiolate (**1AD**) SAMs on Au{111} revealed highly ordered, hexagonally close-packed lattices that were readily displaced by short-chain alkanethiols.[25] The labile nature of **1AD** SAMs has also been exploited to develop an improved soft lithography technique, microdisplacement printing, wherein alkanethiolate ink molecules displace a preexisting **1AD** SAM only in stamped (contacted) regions.[26−29]With this technique, the remaining **1AD** SAM in unstamped areas acts as a diffusion barrier, preventing pattern dissolution. This creates high-quality patterns with sharp edges.

**SCHEME 1: (A) Molecular Structures of 1-Adamantanethiol and 2-Adamantanethiol[a] and (B) Three-Dimensional Representation of the Corresponding Thiolates**

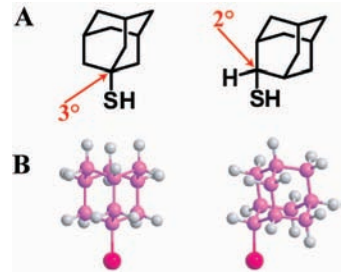


[a] Sulfur attachments to the tertiary (3°) and secondary (2°) carbon on the adamantyl cage in each thiol are shown by the arrows.

The decreased molecular packing density and the lower intermolecular interaction strengths in **1AD** SAMs facilitate their rapid and complete displacement by other thiol molecules at room temperature and at millimolar concentrations.[30−32] By designing the intermolecular interactions, we are able to control the rate and extent of molecular exchange in SAMs, making the microdisplacement printing technique flexible and robust. Here, we demonstrate that 2-adamantanethiol forms well-ordered, hexagonally close-packed monolayers on Au{111} with a c(4 × 2) superlattice. We also show the geometric influence of the adsorbates on the final SAM structure by comparing differences in SAMs of two structural isomers. In 1-adamantanethiol and 2-adamantanethiol, sulfur is attached to the tertiary or secondary carbon, respectively, on the adamantyl cage (Scheme 1). We posit that this alteration changes the orientation of molecules within the respective SAMs, resulting in different superlattice structures. Further, in a 2-adamantanethiolate (**2AD**) monolayer, asymmetry in the adamantyl cage with respect to the gold−sulfur bond axis should modulate the strength of the intermolecular interactions within the SAM, allowing us to control the rate and extent of displacement.

† Part of the "George C. Schatz Festschrift".
‡ Departments of Chemistry and Physics.
§ The Materials Research Institute.
* Address correspondence to this author. E-mail: stm@psu.edu.

10.1021/jp810048n CCC: $40.75 
Published on Web 03/23/2009

## 2. Experimental Methods

**Materials.** The chemicals *n*-dodecanethiol, thiourea, diethyl ether, anhydrous magnesium sulfate, sodium hydroxide, silica gel (70−230 mesh), anhydrous hexanes, potassium thioacetate (KSAc), dimethylformamide (DMF), 2-bromoadamantane (Sigma-Aldrich, St. Louis, MO), 1-bromododecane-$d_{25}$ (Cambridge Isotopes, Andover, MA), and 200-proof ethanol (Pharmco, Brookfield, CT) were used as received. 1-Dodecanethiol-$d_{25}$ was prepared as described previously.[33]

**2-Adamantanethiol Synthesis.** 2-Adamantanethiol was synthesized by modifying a previously reported method[34] using KSAc and 2-bromoadamantane. In a three-necked flask, 10.7 g of 2-bromoadamantane was added to a stirred solution of 10 g of KSAc in 100 mL of DMF. The mixture was refluxed at 130 °C under Ar until 2-adamantanethiol was formed. The resulting solution was allowed to cool to room temperature and was then partitioned between $H_2O$ and hexane; 2-adamantanethiol was extracted into the hexane layer. The resulting extracts were dried over anhydrous magnesium sulfate and evaporated under Ar gas. 2-Adamantanethiol was purified by using flash column chromatography and vacuum sublimation.[35] The purified product was characterized by infrared spectroscopy, nuclear magnetic resonance (NMR), and mass spectroscopy.[36−39] Infrared absorptions in $CCl_4$ were observed at 2910, 2850, 1465, 1455, and 2580 $cm^{-1}$ (S−H, very weak). Nuclear magnetic resonance features in $CDCl_3$ were found as follows: $^1$H NMR $\delta$ 1.41 (d, 1H, $J = 6$ Hz), 1.47 (broad s, 1H), 1.53 (broad s, 1H), 1.72 (broad s, 2H), 1.79 (broad, 8H), 2.15 (broad s, 1H), 2.20 (broad, 1H), and 3.30 (broad d, 1H, $J = 7$ Hz); $^{13}$C NMR $\delta$ 45.90, 36.05, 28.17, 27.37 for primary and tertiary carbons, $\delta$ 39.28, 38.25, 31.27 for secondary carbons. Mass spectral features with assigned fragments and relative intensities were observed at mass/charge ratios of 168 ($C_{10}H_{15}SH^+$, 70%), 135 ($C_{10}H_{15}^+$, 85%), 93 ($C_7H_9^+$, 80%), 91 ($C_7H_7^+$, 90%), 79 ($C_6H_7^+$, 100%), 77 ($C_6H_5^+$, 70%), 67 ($C_5H_7^+$ or $C_{10}H_{15}^{2+}$, 70%), 41 ($C_3H_5^+$, 30%), and 334 ($C_{20}H_{30}S_2^+$, 20%).

**Self-Assembled Monolayer Fabrication.** All **2AD** monolayers were assembled on flame-annealed Au{111} on mica substrates (Agilent Technologies, Tempe, AZ) inserted in 1 mM ethanolic 2-adamantanethiol solution. After annealing the Au substrates with a hydrogen flame, clean substrates were placed in 1 mM 2-adamantanethiol solution either at room temperature for 24 h or at 70 °C for 2 h with subsequent dry-annealing under nitrogen at 78 °C for 17 h in sealed glass v-shaped vials (see the Supporting Information for further details). Following deposition, each sample was removed from solution, rinsed with ethanol, and blown dry with nitrogen 3 times. Displacement of **2AD** SAMs with *n*-dodecanethiol was carried out by immersing preassembled **2AD** SAMs into 1 mM *n*-dodecanethiol solutions for the specified time periods.

**Scanning Tunneling Microscopy.** All STM measurements were performed under ambient conditions with use of a custom-built beetle-style STM.[14,40,41] The samples were scanned within 24 h of fabrication and were stored under nitrogen prior to any other measurements. The **2AD** lattice spacing was measured from Fourier transforms of STM images of **2AD** SAMs after being calibrated using the Fourier transforms of images of the *n*-dodecanethiolate (**C12**) SAM lattice. Lattice spacings were also determined from binary SAMs, which contained distinct ordered domains of both **2AD** and **C12**. In this way, the same tip was used to obtain the lattice spacings of both components simultaneously. The apparent corrugations of the SAMs were calibrated by using the known height of the step edges of the Au{111} substrate in **C12** SAMs.

**X-ray Photoelectron Spectroscopy.** Samples for X-ray photoelectron spectroscopy were stored under nitrogen and transferred to the vacuum chamber within 1 h. Spectra were acquired with a Kratos Axis Ultra photoelectron spectrometer with a monochromatic Al K$\alpha$ source (20 mA, 14 kV), base pressure of $1 \times 10^{-9}$ Torr, and a spot size of 300 $\mu$m × 700 $\mu$m. Survey spectra were acquired at a pass energy of 80 eV and high-resolution spectra of the C 1s, S 2p, and Au 4f regions were collected at a pass energy of 20 eV. The binding energies were referenced to the Au $4f_{7/2}$ peak at 83.98 eV.[42] All of the peaks from the spectra were fit by using Gaussian−Lorentzian (GL) line shapes (CasaXPS analysis software[43]) using a linear background when necessary.

**Cyclic Voltammetry.** A custom-built electrochemical cell[44] and a BAS Epsilon potentiostat (Bioanalytical Systems Inc., West Lafayette, IN) were used to perform electrochemical measurements with methods described previously.[30,32,45] The working electrode was defined by a perfluoroelastomer O-ring (McMaster Carr, Cleveland, OH) mounted on top of the Au{111} substrates inside the electrochemical cell. The area of the working electrode was ~0.1 $cm^2$, electrochemically determined by using the Randle-Sevcik equation.[46]

The potential of the cell was controlled by employing a Ag/AgCl saturated KCl reference electrode (Bioanalytical Systems Inc., West Lafayette, IN) and a Pt wire counter electrode (Bioanalytical Systems Inc., West Lafayette, IN). An aqueous solution of 0.5 M KOH (99.99%, semiconductor grade, Sigma-Aldrich, St. Louis, MO) prepared with deionized water (18.2 MΩ) was used for the supporting electrolyte, after being sparged with ultrahigh purity Ar for 20 min. Cyclic voltammograms were acquired from −200 to −1500 mV at a sweep rate of 20 mV/s and were baseline-corrected by using a straight line subtraction in the first of 100 mV of the sweep in which no faradaic processes occur.[32]

**Infrared Reflection Adsorption Spectroscopy.** All infrared spectra were acquired by using a Nicolet 6700 Fourier transform infrared (FTIR) spectrometer (Thermo Electron Corp., Waltham, MA) equipped with a liquid-nitrogen-cooled mercury−cadmium−telluride detector and a Seagull variable-angle reflection accessory (Harrick Scientific Inc., Pleasantville, NY). The spectrometer was purged with dry $CO_2$-free air prepared by a FTIR Pure Gas Generator (Parker-Balston, Cleveland, OH). The data were collected at grazing incidence reflection (82° relative to surface normal) with *p*-polarized light and a mirror speed of 1.27 cm/s with a resolution of 2 $cm^{-1}$. All SAM spectra were transformed by using N−B Medium apodization and were normalized with data recorded for perdeuterated *n*-dodecanethiolate monolayers on Au{111}. Spectra were acquired for each **2AD** SAM to verify the absence of impurities and the presence of the characteristic $CH_2$ stretch at 2913 ± 1 $cm^{-1}$, which is indicative of well-ordered **2AD** SAMs. The samples were placed in 1 mM ethanolic *n*-dodecanethiol solutions for displacement. After every specified time frame, the SAMs were rinsed with ethanol and blown dry with nitrogen. Each FTIR spectrum was recorded, and the sample was returned to the *n*-dodecanethiol solution for further exposure. In the case of **DA 2AD** SAM displacement, the displacement interval was increased as the rate of change diminished. To achieve saturation coverage, the samples were placed in a *n*-dodecanethiol solution for a total of 24 h to allow additional growth and ordering. Subsequently, a final spectrum was recorded for each sample to determine the saturation coverage.

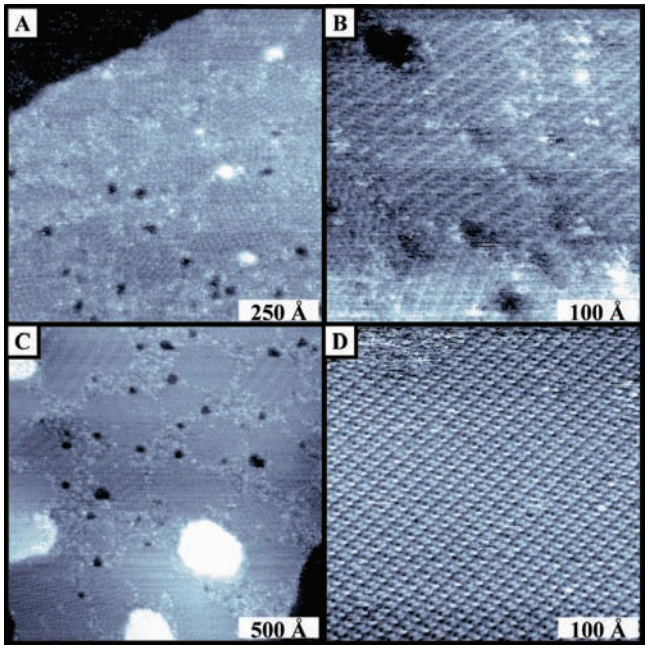


**Figure 1.** Scanning tunneling microscopy images of 2-adamantanethiolate (**2AD**) self-assembled monolayers (SAMs) on Au{111} fabricated by immersing substrates in 1 mM 2-adamantanethiol solution at room temperature for 24 h (**RT 2AD** SAMs, A and B) or by first exposing clean Au substrates to solution at 70 °C for 2 h, then dry-annealing the samples under nitrogen at 78 °C for 17 h (**DA 2AD** SAMs, C and D); sample bias 0.80 V, tunneling current 2.0 pA. The round features with high contrast in panel C correspond to Au adatom islands with measured heights of 2.4 Å, consistent with the Au{111} single-atom step height.[55]

## 3. Results and Discussion

**Characterization of 2-Adamantanethiolate SAMs on Au{111}.** Molecular exchange with a SAM strongly depends upon the defect densities and domain sizes of the films.[14,31,47] Thus, we first established conditions for controlling domain sizes (and thus defect densities) in **2AD** SAMs. Small-domain **2AD** SAMs with higher defect densities were prepared by placing clean Au{111} substrates in 1 mM ethanolic 2-adamantanethiol solution at room temperature (**RT**) for 24 h (**RT 2AD** SAMs, Figure 1, parts A and B). Large-domain **2AD** SAMs with lower defect densities were fabricated by first placing clean Au substrates in 1 mM ethanolic 2-adamantanethiol solution at 70 °C for 2 h, then dry-annealing (**DA**) the samples under nitrogen at 78 °C for 17 h (**DA 2AD** SAMs, Figure 1, parts C and D). The samples prepared from solution at 70 °C formed **2AD** SAM surfaces with greater degrees of long-range order than the samples prepared at room temperature. Other temperatures (50 and 60 °C) accelerate ordering. Annealing at 78 °C gives further access to slow ordering, extending to large domains. The annealing time used is not critical; however, we observed evidence of desorption or oxidation including molecular vacancies, disorientation, or disordering and clustering for annealing times over 17 h (Figure S1 in the Supporting Information).[48,49] As shown in Figure 1, domain boundaries in STM images appear as slight protrusions. The domain sizes of **RT 2AD** SAMs were observed to be <200 Å, with a large number of disordered molecules in domain boundaries, vacancy islands, and step edges (Figure 1A). High-resolution STM images of **RT 2AD** SAMs (e.g., Figure 1B) reveal distinct domain boundaries separating rotational domains. In contrast, annealing at a moderately elevated temperature (78 °C) results in **2AD** SAMs with larger domain sizes, typically >500 Å across,

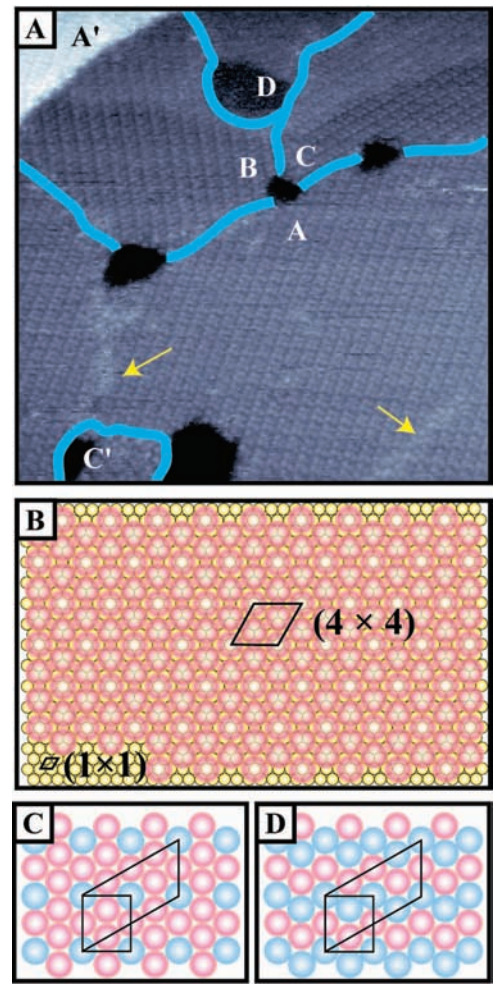


**Figure 2.** (A) A scanning tunneling microscopy image of a 2-adamantanethiolate (**2AD**) self-assembled monolayer (SAM) on Au{111} showing several rotational domains. The SAM was prepared by first placing a Au substrate in a 1 mM 2-adamantanethiol solution at 70 °C for 2 h, then dry-annealing the sample under nitrogen at 78 °C for 17 h (**DA 2AD** SAM). The lattice in domain B is rotated 30° counterclockwise with respect to domain A, and domain C is rotated 40° clockwise with respect to domain A. The domains A′ and C′ have the same orientations as domains A and C, respectively. Domain D is disordered. The yellow arrows denote translational domain boundaries; 600 Å × 600 Å; sample bias 0.80 V, tunneling current 2.0 pA. (B) The proposed unit cell for the **2AD** lattice on Au{111}. (C and D) The proposed superlattice c(4 × 2) structures of alternating heights resulting from different phases ($\beta$ and $\delta$), respectively.[56]

and a substantial decrease in disordered regions and vacancy islands (Figure 1C).[14,50−54] During annealing, thermal energy allows molecules in disordered regions to change orientation, forming highly ordered monolayers over large areas (Figure 1D). However, disordered regions still remain proximate to vacancy islands, between domains, and along step edges (Figure S1 in the Supporting Information).

In molecularly resolved images, we observe that rows of molecules change direction between domains, even without apparent depressions or protrusions at rotational domain boundaries. The relative orientation angles between rotational domains were measured, although the exact rotation with respect to the underlying Au substrate cannot be determined by imaging only the adlayer. Figure 2A shows four rotational domains in a **DA 2AD** SAM. Slight apparent protrusions observed in region A (arrows in Figure 2A) indicate translational domain boundaries in the same rotational domain.[4] The relative rotational

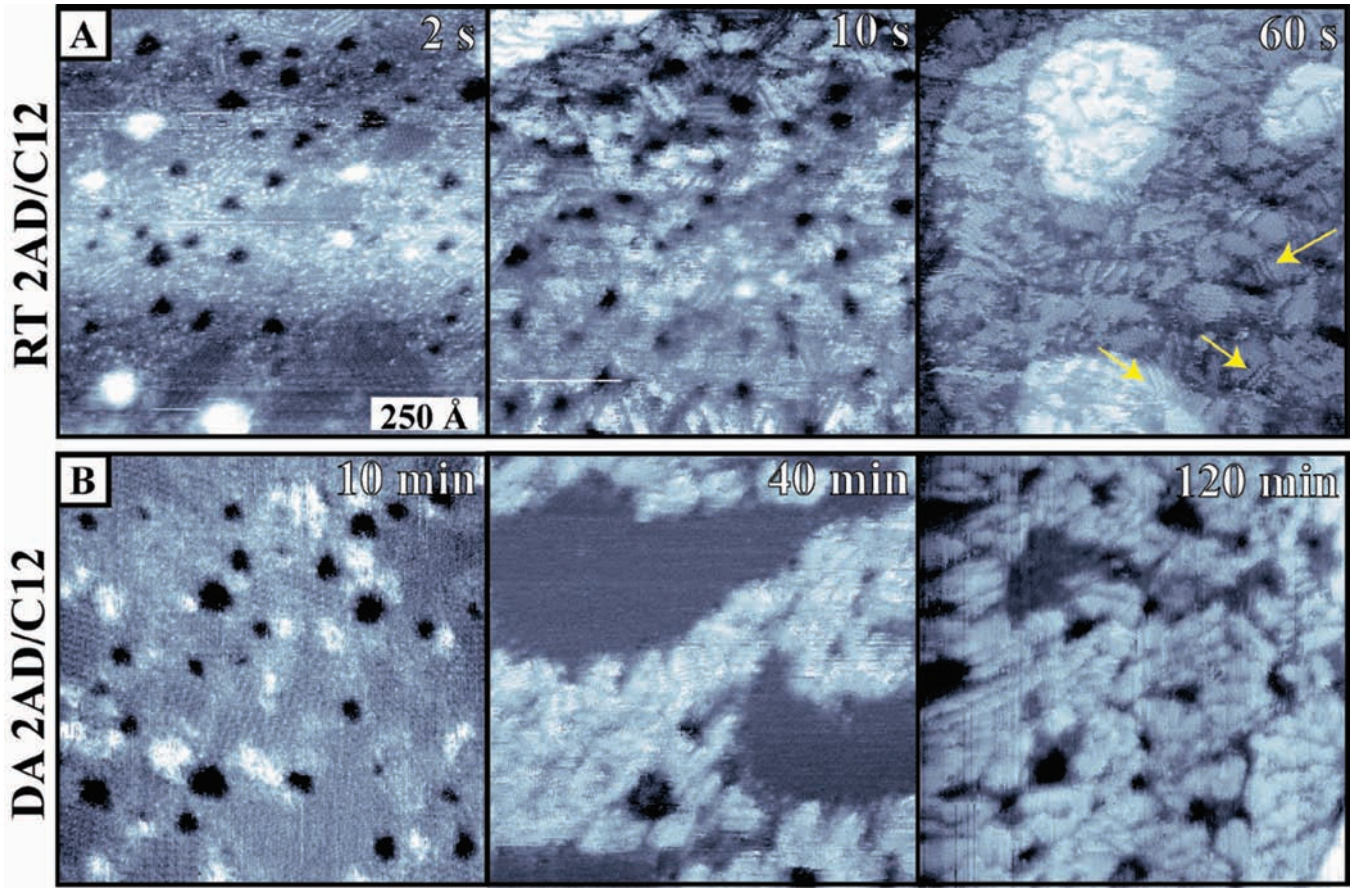


**Figure 3.** (A and B) Scanning tunneling microscopy images of mixed SAMs containing 2-adamantanethiolate (**2AD**) and *n*-dodecanethiolate (**C12**) domains fabricated by inserting **2AD** SAMs in 1 mM *n*-dodecanethiol solution for the specified times. (A) The **2AD** SAMs were prepared by immersing clean Au substrates in 1 mM 2-adamantanethiol solution at room temperature for 24 h (**RT 2AD** SAMs). The small protruding features in the first image correspond to Au adatom islands formed during **2AD** self-assembly.[55] (B) The **2AD** SAMs were prepared by first placing Au substrates in 1 mM 2-adamantanethiol solution at 70 °C for 2 h, then dry-annealing the samples under nitrogen at 78 °C for 17 h (**DA 2AD** SAMs); sample bias 0.80 V, tunneling current 2.0 pA.

angles of domains B and C were measured from domain A; the angle for domain D was not measured due to disorder. The angle from domain A to domain B was 30° counterclockwise, whereas the angle from domain A to domain C was 40° clockwise. Other rotational domains were also observed in other STM images. All measured rotational angles between domains were close to 30°, within a standard deviation of 10° due to errors resulting from thermal drift in our ambient STM. The restricted variation in relative rotational angles between domains in **2AD** SAMs is consistent with our proposed lattice structure (vide infra).

Individual molecules in **2AD** SAMs are arranged in a hexagonally close-packed formation with a c(4 × 2) superlattice structure (Figure S2 in the Supporting Information).[5,56,57] The distance between hexagonal points in reciprocal space corresponds to measured nearest neighbor distances of 6.9 ± 0.4 Å and next nearest neighbor distances of 11.6 ± 0.4 Å, which are close to the nearest neighbor distances of 6.67 ± 0.01 Å for three-dimensional adamantane crystals.[58] On the basis of the above observations, we propose that the most likely unit cell assignment is (4 × 4) with respect to the Au{111} substrate, as shown in Figure 2B.[19] Using a gold spacing of 2.88 Å, a (4 × 4) unit cell has a lattice constant of 11.52 Å and comprises three molecules per unit cell. The phases of the c(4 × 2) superlattice with respect to the proposed (4 × 4) unit cell observed in **2AD** SAMs are $\beta$ and $\delta$ phases,[59] consisting of molecules with two different apparent heights (Figure 2C,D). We observed ellipsoids at molecular resolution and linear features in large scanning areas (Figure 1) depending on the tip condition. This might have been caused by the convolution of c(4 × 2) phases or different molecular interactions between molecules driven by the flexible molecular orientation of **2AD** (e.g., tilt or twist).[21,23] However, it was not possible to determine tilt or twist angles of the adamantyl cage from the Au−S bond axis by STM.

**Displacement of 2-Adamantanethiolate SAMs with *n*-Dodecanethiol.** Scanning tunneling microscopy allows us to monitor the molecular exchange of **2AD** monolayers with other alkanethiols at the nanoscale. Figure 3 shows STM images of **2AD** SAMs containing **C12** domains generated by displacement with 1 mM ethanolic *n*-dodecanethiol solution. To correlate exchange kinetics with the domain sizes and defect densities in **2AD** SAMs, both **RT 2AD** and **DA 2AD** SAMs were immersed in 1 mM ethanolic *n*-dodecanethiol solutions for controlled time periods. Figure 3 A shows the results of displacement of **RT 2AD** SAMs by **C12** for 2, 10, and 60 s from left to right. Figure 3B depicts the displacement of **DA 2AD** SAMs by **C12** for 10, 40, and 120 min from left to right.

As expected, small-domain **RT 2AD** SAMs undergo much faster molecular exchange with **C12** than large-domain **DA 2AD** SAMs. After 2 s of displacement, the remaining lower areas correspond to well-ordered **2AD** domains, while the dots and lines with high contrast are assigned as less-ordered **C12** molecules. In the early stages of displacement, rapid molecular exchange primarily occurs in disordered regions such as domain

boundaries, vacancy islands, and step edges;[60] adsorbed **C12** molecules in these regions are disordered. After 10 s of displacement, corrugated rod-like structures begin to appear in the SAM, oriented in different directions; we attribute these features to the **C12** areas that displace ordered **2AD** molecules in different rotational domains. After 60 s of displacement, **C12** molecules start forming small domains of hexagonally close-packed lattices; well-organized **2AD** domains were still present (not shown). We ascribe depressed lines observed in some **C12** regions (arrows in Figure 3A) to missing rows caused by the size disparity between **C12** and **2AD** after exchange. During the displacement process, a **C12** molecule replaces a relatively large **2AD** molecule, leaving room for additional **C12** insertion. This lattice mismatch is a key feature of successful and complete displacement.[31] More **C12** molecules eventually backfill these rows, optimizing hexagonal close-packing. As insertion time increased, the fraction of the surface covered by **2AD** domains decreased and displacement was essentially complete after 40 min. At very long displacement times, molecular exchange continued at the boundaries between **C12** islands until they eventually coalesced into large domains.[32]

As expected, the more ordered **DA 2AD** SAMs with larger domain sizes exhibit slower **C12** exchange kinetics. The displacement process for **DA 2AD** SAMs was much slower than that for **RT 2AD** SAMs (Figure 3B). However, the initial rapid molecular exchange of disordered **2AD** regions also occurred quickly (first image of Figure 3B). At longer exchange times, the difference in kinetics is evident; even after 40 min of insertion in *n*-dodecanethiol solution, **DA 2AD** SAMs still contained large, well-ordered **2AD** domains, and 120 min was required to cover most of the surface with **C12**.

Important differences are observed between the displacement of SAMs of **2AD** and SAMs of its structural isomer, **1AD**. The **C12** regions in mixed SAMs formed by the short-time displacement of **RT 2AD** SAMs showed rod-like structures that grew linearly (see Figure 3A). In contrast, alkanethiolate regions resulting from the solution displacement of **1AD** SAMs with *n*-octanethiol, *n*-decanethiol, and *n*-dodecanethiol appear as clusters of molecules that grow radially.[25,31,32] The different growth patterns of **C12** domains in **2AD** SAMs suggest their displacement mechanism is not precisely the same as the displacement in **1AD** SAMs; we attribute this to the different lattice structures of the original labile SAMs.

Apparent height differences in mixed **2AD/C12** SAMs can be used to infer the apparent height of the **2AD** monolayer. The apparent heights are used along with the lattice spacings (and surface coverages) to help identify molecules in mixed monolayers.[14,61−64] Figure 4 shows STM images of a binary SAM composed of both **2AD** and **C12** domains, fabricated by 40 min of displacement of a **DA 2AD** SAM in 1 mM *n*-dodecanethiol solution. In Figure 4A, the low-contrast depressed areas correspond to **2AD** domains and the high-contrast protruding patches correspond to **C12** domains. The measured apparent height differences between **2AD** and **C12** are 3.5 ± 0.2 Å. On the basis of the previously measured apparent height of **C12** regions as 12.0 ± 0.2 Å,[62] the measured apparent height of **2AD** SAMs under these conditions should be 8.7 ± 0.2 Å.

Figure 4B shows a highly ordered mixed SAM with **2AD** and **C12** domains, in good agreement with the expectation that well-ordered **2AD** domains are strongly resistant to **C12** exchange. On careful inspection, **C12** regions consist of several rotational domains, attributed to separate nucleation of these domains during displacement (Figure 4C). At high resolution (Figure 4D), **C12** domains show individual **C12** molecules in a hexagonally close-packed lattice in addition to the aforementioned linear patterns.

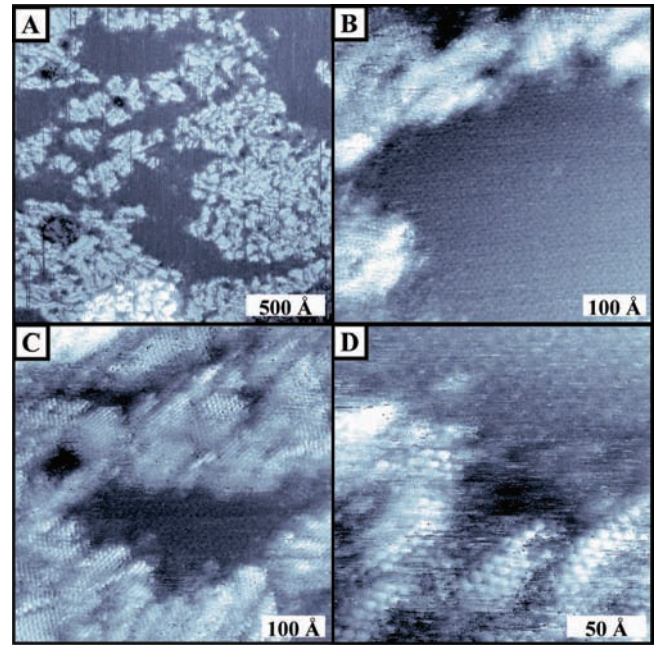


**Figure 4.** (A−D) Scanning tunneling microscopy images of a mixed SAM composed of 2-adamantanethiolate (**2AD**) and *n*-dodecanethiolate (**C12**) domains on Au{111} fabricated by inserting a **2AD** SAM into a 1 mM *n*-dodecanethiol solution. The **2AD** SAM was prepared by first placing a Au substrate in 1 mM 2-adamantanethiol solution at 70 °C for 2 h, then dry-annealing the sample under nitrogen at 78 °C for 17 h (**DA 2AD** SAM); sample bias 1.0 V, tunneling current 2.0 pA.

After displacement reaches completion, the predominant **C12** phase is the saturated phase where the linear hydrocarbon chains are aligned with a $(\sqrt{3} \times \sqrt{3})R30°$ lattice. However, at shorter displacement times, other **C12** SAM phases were observed. Figure 5 shows STM images of **C12** domains after 60 min of exchange with a **DA 2AD** SAM. These phases resemble those previously observed for low-coverage *n*-alkanethiolate SAMs.[65−68] Unsaturated striped phases of linear alkyl chains known as $\delta$ and $\chi$ phases (see in Figure 5A) are initially formed and are eventually replaced by a saturated $\phi$ phase (Figure 5B) upon continued exposure. We propose that molecular exchange between **2AD** and **C12** occurs initially at a 1:1 ratio,[69−71] resulting in unsaturated phases due to the size disparity between **2AD** and **C12**, and that vacancies are later backfilled by additional **C12** molecules.

**Intermolecular Interaction Strengths and Molecular Packing in 2-Adamantanethiolate SAMs.** Weak intermolecular interactions and low molecular packing density in **1AD** SAMs were the main thermodynamic driving forces for displacement by *n*-alkanethiols.[30,32] These two factors for **2AD** monolayers were quantified by using cyclic voltammetry and X-ray photoelectron spectroscopy (XPS). Samples for these experiments were prepared in the same way as those used for STM studies.

The cathodic peak potential ($E_p$) in cyclic voltammetry offers insight into the strength of intermolecular interactions in SAMs.[72−77] Figure 6 shows representative voltammograms of single-component **1AD**, **2AD**, and **C12** SAMs. Respective average $E_p$, cathodic peak current ($I_p$), peak area, and the full-width-at-half-maxima (fwhm) from several voltammograms are listed in Table 1. The one-electron reductive desorption of the thiolate from the gold electrode generates the cathodic peaks in the voltammograms. As shown in Table 1, the average $E_p$

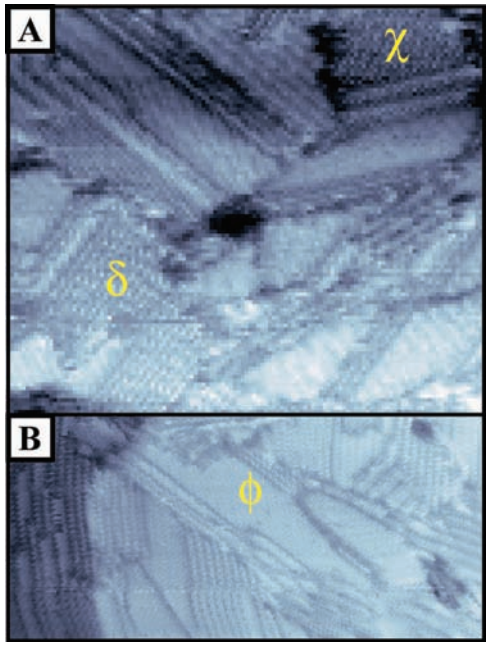


**Figure 5.** Scanning tunneling microscopy images of *n*-dodecanethiolate (**C12**) phases generated from displacement of a 2-adamantanethiolate (**2AD**) SAM with a 1 mM *n*-dodecanethiol solution for 60 min: (A) 715 Å × 615 Å; (B) 996 Å × 477 Å; sample bias 1.0 V, tunneling current 2.0 pA. The **2AD** SAM was fabricated by first placing a Au substrate in 1 mM 2-adamantanethiol solution at 70 °C for 2 h, then dry-annealing the sample under nitrogen at 78 °C for 17 h (**DA 2AD** SAM).

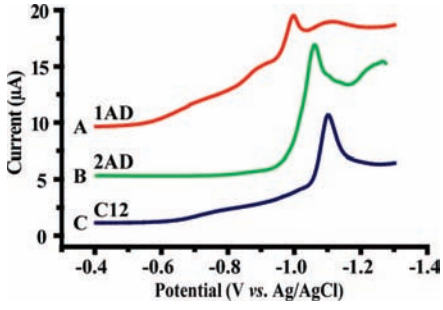


**Figure 6.** Representative voltammograms showing the reductive desorption of (A) a single-component 1-adamantanethiolate (**1AD**) SAM, (B) a single-component 2-adamantanethiolate (**2AD**) SAM, and (C) a single-component *n*-dodecanethiolate (**C12**) SAM. Baseline correction was applied to account for solution resistance and sample/electrode contact resistance using a straight line subtraction in the first of 100 mV of the sweep in which no faradaic processes occur.[32] The traces are offset for clarity.

for single-component **2AD** SAMs appeared at −1076 ± 12 mV, which is slightly more positive than the average $E_p$ for **C12** SAMs (−1113 ± 9 mV),[78] but far more negative than that observed for **1AD** SAMs (−996 ± 4 mV).[30] A more positive $E_p$ for the SAM implies that less energy is required to desorb each molecule reductively from the Au surface. Since the Au−S bond strength is similar for the three species described here, this suggests that the intermolecular interactions in **2AD** SAMs are weaker than those in **C12** SAMs, but are apparently stronger than those in **1AD** SAMs. The asymmetry in the adamantyl cage with respect to the Au−S bond provides a degree of freedom to **2AD** molecules, which evidently leads to stronger intermolecular interactions, perhaps due to different intermolecular distances of closest approach. The larger standard deviation of the average $E_p$ for **2AD** SAMs may be caused by disordered regions in **2AD** SAMs.[79] The very narrow fwhm of the cathodic peak in **2AD** SAMs may also reflect increased intermolecular interaction strengths relative to **1AD** SAMs.[80,81]

**TABLE 1: Average Cathodic Peak Potential ($E_p$), Current ($I_p$), Area, and Full-Width-at-Half-Maxima (fwhm) from Voltammograms of Single-Component 1-Adamantanethiolate (1AD) SAMs, Single-Component 2-Adamantanethiolate (2AD) SAMs, and Single-Component *n*-Dodecanethiolate (C12) SAMs[a]**

| | avg peak potential (mV) | avg peak current (μA) | avg peak area (μC) | avg peak fwhm (mV) |
|---|---|---|---|---|
| **1AD** | −996 ± 4 | 3.2 ± 0.4 | 8.5 ± 1.8 | 58 ± 11 |
| **2AD** | −1076 ± 12 | 5.0 ± 0.7 | 9.3 ± 3.0 | 35 ± 8 |
| **C12** | −1113 ± 9 | 6.0 ± 1.0 | 14.2 ± 0.8 | 45 ± 9 |

[a] All SAMs were prepared by immersing clean Au substrates in the corresponding 1 mM ethanolic thiol solutions at room temperature for 24 h.

The **C12/2AD** ratios for both the $I_p$ (1.2) and the cathodic peak area (1.5) reflect the differences in molecular packing density between **C12** and **2AD** SAMs, since each molecule loses one electron during electrochemical desorption.[32,45] The smaller average $I_p$ and cathodic peak area for **2AD** SAMs on Au{111} compared to **C12** SAMs indicate that the absolute surface coverage (number of molecules per unit area) of **2AD** SAMs is lower than that for **C12** SAMs. If we consider only the unit cell of each SAM, a **C12** SAM (one molecule in a $(\sqrt{3} \times \sqrt{3})R30°$ unit cell) contains 1.8 (16/9) times more molecules in the same area as a **2AD** SAM (three molecules in a (4 × 4) unit cell).[45] However, disordered molecules in the **2AD** SAMs strongly influence the uncertainty in the $I_p$ and the peak area, making direct comparisons difficult. Also, the larger average $I_p$ and peak area of **2AD** SAMs than those of **1AD** SAMs indicate that the average number of molecules per unit area of **2AD** SAMs is slightly higher than that for **1AD** SAMs. This can be rationalized by the difference of intermolecular distances between **2AD** SAMs (6.65 Å) and **1AD** SAMs (6.72 or 6.87 Å).[19]

Changes in XPS spectra of the mixed **2AD/C12** SAMs generated by displacement compared to single-component **2AD** and **C12** SAMs allow us to quantify the extent of displacement in exchange reactions and to monitor the change in local electronic properties of the interface between the organic layer and the underlying Au substrate. Importantly, this technique provides us with an ensemble measurement to complement the molecular-scale information obtained by STM. Figure 7 shows the C 1s region of the XPS spectra for single-component **2AD** and **C12** SAMs, as well as binary **2AD/C12** SAMs created by the displacement of **RT 2AD** SAMs with a 1 mM *n*-dodecanethiol solution for 10 s, 1 min, and 10 min. All C 1s spectra for each sample were calibrated by using the Au $4f_{7/2}$ peak at 83.98 eV. The Au photoelectron peaks for each sample (not shown) did not change in shape or fwhm, indicating that these electrons come from the bulk gold.[23] The C 1s peaks from the spectra of the mixed **2AD/C12** SAMs shift from the lower **2AD** binding energy to the higher **C12** binding energy as the exposure time increases (see Table 2); a similar trend is observed for **DA 2AD** SAMs at long displacement times.

For each **2AD** SAM measurement, the observed peak is a convolution of two peaks, with an area ratio of approximately 9:1 (inset in Figure 7). The smaller peak component at 285.0 ± 0.1 eV corresponds to the carbon with the thiol substituent. The larger peak component at 283.8 ± 0.1 eV corresponds to the other nine adamantyl carbons.[30] These peaks are different than the **C12** peak positions of 286.5 ± 0.1 and 284.9 ±

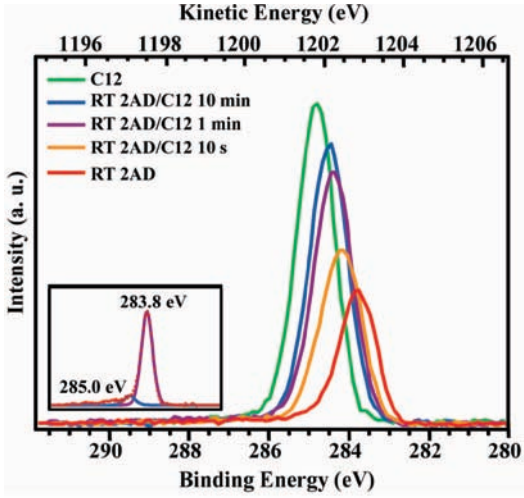


**Figure 7.** The C 1s region of XPS spectra of a single-component 2-adamantanethiolate (**2AD**) SAM, a single-component *n*-dodecanethiolate (**C12**) SAM, and binary **2AD/C12** SAMs created by displacement of **2AD** SAMs with 1 mM *n*-dodecanethiol solution for 10 s, 1 min, and 10 min. The **2AD** SAMs were prepared by inserting Au substrates in 1 mM 2-adamantanethiol solution at room temperature for 24 h (**RT 2AD** SAMs). The inset shows the C 1s peak of a single-component **RT 2AD** SAM fit by two Gaussian−Lorentzian line shapes with maxima at 283.8 and 285.0 eV (283.9 and 285.1 eV for a dry-annealed **2AD** SAM, see Figure S3 in the Supporting Information), and with a peak area ratio of 9:1.

**TABLE 2: Binding Energies and the Full-Width-at-Half-Maxima (fwhm) of the C 1s Peaks in the XPS Spectra of Single-Component 2-Adamantanethiolate (2AD) SAMs, Single-Component *n*-Dodecanethiolate (C12) SAMs, and Mixed 2AD/C12 SAMs Created by Displacement of 2AD SAMs in 1 mM *n*-Dodedcanethiol Solution for the Specified Times[a]**

| | C 1s binding energy (eV) | C 1s fwhm (eV) | molecular species (%)[b] | |
|---|---|---|---|---|
| | | | **2AD** | **C12** |
| **RT 2AD** | 283.8 | 1.09 | 100 | 0 |
| **RT 2AD** 10 s | 284.2 | 1.19 | 70 | 30 |
| **RT 2AD** 1 min | 284.4 | 1.15 | 31 | 69 |
| **RT 2AD** 10 min | 284.5 | 1.13 | 20 | 80 |
| **C12** | 284.9 | 1.11 | 0 | 100 |
| **DA 2AD** | 283.9 | 1.00 | 100 | 0 |
| **DA 2AD** 10 min | 284.3 | 1.19 | 65 | 35 |
| **DA 2AD** 40 min | 284.4 | 1.21 | 51 | 49 |
| **DA 2AD** 120 min | 284.5 | 1.24 | 43 | 57 |
| **C12** | 284.9 | 1.11 | 0 | 100 |

[a] The **2AD** SAMs were prepared by immersing clean Au substrates in 1 mM 2-adamantanethiol solution at room temperature for 24 h (**RT 2AD** SAMs) or by placing Au substrates in 2-adamantanethiol solution at 70 °C for 2 h, then dry-annealing the samples under nitrogen at 78 °C for 17 h (**DA 2AD** SAMs). [b] Surface fraction of each molecule, estimated from the area ratios of the individual peaks discussed in the text.

0.1 eV.[82,83] The larger intensity, lower binding-energy peak corresponds to the **C12** hydrocarbon tail. The lower binding energy of the C 1s peak in a single-component **2AD** SAM relative to a single-component **C12** SAM is attributed to the adamantyl cage structure rather than chemical shift.[23] This binding energy difference is substantially larger than typically observed chemical shifts (usually 0.1−0.3 eV) and the C 1s peak moves closer to the C 1s binding energies found for graphite and diamond.[42,84,85] The binding energy of the C 1s peak from **2AD** SAMs, 283.8 ± 0.1 eV, is slightly lower than that for **1AD** SAMs, 284.4 ± 0.1 eV.[30] This could originate from the structural flexibility of the molecule caused by tilting or twisting for stronger intermolecular interactions. On the basis of previous results and discussions,[23] 2-adamantanethiolates on Au{111} may be in a more tilted orientation rather than upright on the surface. Interestingly, the C 1s binding energy range of **DA 2AD** SAMs (283.9−284.0 eV) is slightly higher than that for **RT 2AD** SAMs (283.7−283.8 eV), which we attribute to the different local environment in the SAM (Figure S3 in the Supporting Information). We infer that better ordering on large scales gives higher C1s binding energy.

The coverages of **2AD** and **C12** domains in binary SAMs were estimated from the peak areas of the C 1s region of the XPS spectra and are given in Table 2. The coverage of each molecule in binary SAMs was determined by comparing the peak areas of the mixed monolayers to those of the single-component **2AD** and **C12** SAMs. Calculations using Gaussian−Lorentzian fits to the spectra for the original monolayers were not applicable,[30] due to the changes in the work functions of the local surface.[86] These changes can be directly observed by the change in the C 1s peak positions for mixed **2AD/C12** SAMs vs **2AD** SAMs while maintaining similar peak widths. As shown in Table 2, the displacement of **DA 2AD SAMs** with **C12** is much slower compared to that of **RT 2AD** SAMs, principally resulting from the higher SAM quality—large domain sizes and fewer defects. Another factor is higher molecular coverage indicated by the relatively larger C 1s peak area in **DA 2AD** SAM (Figure S3 in the Supporting Information).

**Kinetics of Displacement in 2-Adamantanethiolate SAMs.** We utilized Fourier transform infrared (FTIR) spectrometry to monitor the SAM displacement reactions through completion, and thus the quantitative kinetics of solution displacement of **2AD** SAMs by **C12**. Grazing incidence FTIR spectra of **2AD** and **C12** SAMs were obtained from 800 to 4000 $cm^{-1}$. Characteristic spectra of each adsorbate are shown in Figure 8A. The **2AD** spectra display two main peaks and two shoulders attributed to C−H stretching in the region from 2750 to 3050 $cm^{-1}$. The 2850 and 2913 $cm^{-1}$ peaks are associated with symmetric and asymmetric $CH_2$ stretch modes, respectively.[31,87] The shoulders at 2899 and 2934 $cm^{-1}$ are associated with C−H stretches.[87−89] The $CH_2$ symmetric and asymmetric stretch modes of the **C12** spectra were positioned at 2850 and 2919 $cm^{-1}$, nearly overlapping those of **2AD** in the same spectral region. The $CH_3$ symmetric and asymmetric stretches were resolved well at 2877 and 2963 $cm^{-1}$, respectively.[83]

The displacement of **2AD** SAMs by **C12** was studied by monitoring the emergence of the well-resolved 2877 $cm^{-1}$ $CH_3$ symmetric stretch as a function of *n*-dodecanethiol solution exposure time.[28,31,90] Both **RT 2AD** and **DA 2AD** SAMs were prepared and immersed in 1 mM ethanolic *n*-dodecanethiol solution for the specified time periods. The process was interrupted between time intervals for analysis by FTIR and samples were then returned to the *n*-dodecanethiol solution for the next displacement cycle. Figure 8B shows the spectral evolution of a **DA 2AD** SAM at representative time intervals (1, 10, 40, and 180 min) during displacement. After 180 min of exposure, the sample was left in solution for a total of 24 h to reach saturation. The final spectrum was collected in order to determine the maximum **C12** coverage. The fractional coverage of **C12** was determined by taking the ratio of the interval and final peak area of the 2877 $cm^{-1}$ $CH_3$ symmetric stretch of **C12**. Figure 8C shows the **C12** coverage as a function of displacement time for the **RT 2AD** and **DA 2AD** SAMs. As a result, **RT 2AD** SAMs were rapidly displaced, approaching

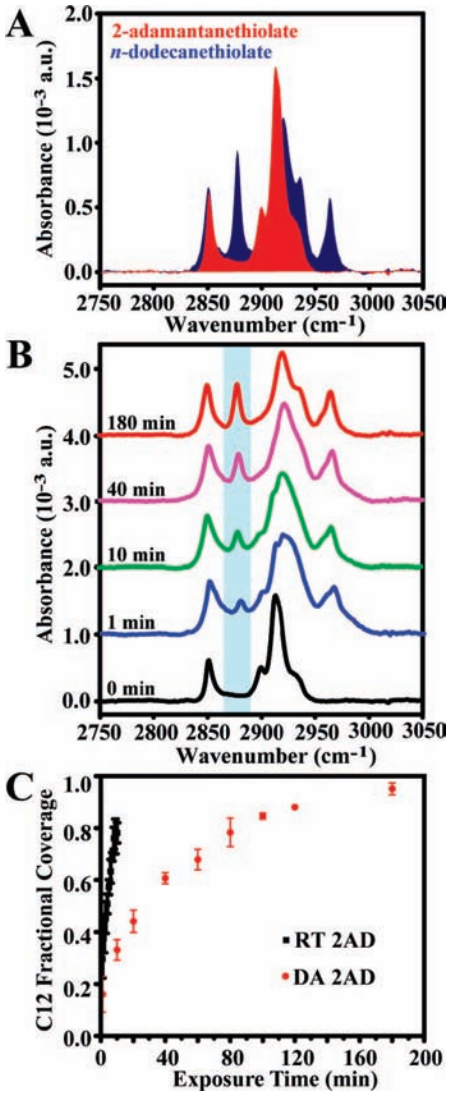


**Figure 8.** (A) Infrared spectra of the C−H stretch region of a 2-adamantanethiolate (**2AD**) SAM and a *n*-dodecanethiolate (**C12**) SAM, showing their spectral overlap (see text for mode assignments). The **2AD** SAMs were prepared either by inserting clean Au substrates in 1 mM 2-adamantanethiol solution at room temperature for 24 h (**RT 2AD** SAMs) or by placing Au substrates in 2-adamantanethiol solution at 70 °C for 2 h, then dry-annealing the samples under nitrogen at 78 °C for 17 h (**DA 2AD** SAMs). (B) Spectral evolution of a **DA 2AD** SAM displaced by **C12** in 1 mM solution as a function of immersion time, 1, 10, 40, and 180 min. (C) Plot of **C12** monolayer coverage formed by displacement of **RT 2AD** and **DA 2AD** SAMs by **C12** as a function of the specified periods of displacement time, at every 1 min interval for **RT 2AD** SAMs, and at 1, 10, 20, 40, 60, 80, 100, 120, and 180 min intervals for **DA 2AD** SAMs.

saturation with **C12** in less than 20 min. However, **DA 2AD** SAMs were replaced by **C12** more slowly, requiring over 180 min to approach completion. Both results are consistent with the STM images and C 1s XPS spectral analyses.

As explained above, displacement is driven by three major factors: access to the substrate at defect sites susceptible to insertion and island nucleation, lower density of Au−S bonds relative to the displacing alkanethiolate SAM, and lattice mismatch that allows the SAM to continue to completion.[30,31,91,92] While the internal domain structures of **RT 2AD** and **DA 2AD** SAMs are identical, we observed significant differences in the defect densities and the domain sizes for the two preparations (vide supra). Manipulating these factors, via annealing, influences the overall displacement process. Numerous defect sites and disordered regions in **RT 2AD** SAMs allow rapid exchange, while the improved quality of **DA 2AD** SAMs in terms of ordering, domain sizes, and smooth domain boundaries limit exchange, resulting in slower overall rates of displacement.

## 4. Conclusions

The study of **2AD** SAMs with STM offers insight into the relationships between molecular geometry and intermolecular interactions in SAMs. In **2AD** SAMs, the different position of sulfur on the adamantyl cage changes the orientations of the molecules on the surface as well as the Au−S bond configuration in comparison with previously reported **1AD** SAMs. This results in stronger and directional intermolecular interactions, which also affect substrate−molecule interactions. In the molecular exchange between **2AD** SAMs and *n*-dodecanethiols in solution, the c(4 × 2) molecular arrangement directs the linear growth of **C12** domains during initial displacement, which modulates the local work function of mixed SAMs. Increased intermolecular interactions in the ordered **2AD** domains result in resistance to displacement by **C12**. Significantly, the kinetics of molecular exchange in **2AD** SAMs can be tuned by changing the domain sizes and densities of disordered molecules. The different kinetics and structures of these SAMs offer control over molecular exchange and also indicate the importance of directional interactions in patterning surfaces at the nanoscale.

**Acknowledgment.** This research has been supported by the Center for Nanoscale Science, a National Science Foundation Materials Research and Science Engineering Center, and the Semiconductor Research Corporation. We thank the Pennsylvania State University Materials Characterization Laboratory and the Pennsylvania State University node of the National Nanotechnology Infrastructure Network for the use of the Kratos XPS system. We especially thank Dr. Jaehong Seo for synthetic aid and characterization of 2-adamantanethiol. Also, Dr. Shelley A. Claridge, Dr. Thomas J. Mullen, and Héctor M. Saavedra are acknowledged for fruitful discussions. This paper is dedicated to Prof. George C. Schatz, who has served as a mentor, a friend, and an inspiration.

**Supporting Information Available:** STM images showing the disordered regions in **DA 2AD** SAMs at different annealing times, molecular-resolution STM images of **2AD** SAMs with Fourier transforms, the magnified C 1s region of XPS spectra of both **RT 2AD** and **DA 2AD** SAMs, and the sulfur regions of XPS spectra of single-component **RT 2AD**, **DA 2AD**, **C12** SAMs and mixed **2AD/C12** SAMs. This material is available free of charge via the Internet at http://pubs.acs.org.

## References and Notes

(1) Dubois, L. H.; Nuzzo, R. G. *Annu. Rev. Phys. Chem.* **1992**, *43*, 437.
(2) Nuzzo, R. G.; Allara, D. L. *J. Am. Chem. Soc.* **1983**, *105*, 4481.
(3) Noh, J.; Hara, M. *Langmuir* **2002**, *18*, 1953.
(4) Poirier, G. E. *Chem. Rev.* **1997**, *97*, 1117.
(5) Poirier, G. E.; Tarlov, M. J. *Langmuir* **1994**, *10*, 2853.
(6) Love, J. C.; Estroff, L. A.; Kriebel, J. K.; Nuzzo, R. G.; Whitesides, G. M. *Chem. Rev.* **2005**, *105*, 1103.
(7) Smith, R. K.; Lewis, P. A.; Weiss, P. S. *Prog. Surf. Sci.* **2004**, *75*, 1.
(8) Bent, S. F. *ACS Nano* **2007**, *1*, 10.
(9) Smith, R. K.; Nanayakkara, S. U.; Woehrle, G. H.; Pearl, T. P.; Blake, M. M.; Hutchison, J. E.; Weiss, P. S. *J. Am. Chem. Soc.* **2006**, *128*, 9266.
(10) Anderson, M. E.; Smith, R. K.; Donhauser, Z. J.; Hatzor, A.; Lewis, P. A.; Tan, L. P.; Tanaka, H.; Horn, M. W.; Weiss, P. S. *J. Vac. Sci. Technol. B* **2002**, *20*, 2739.

(11) Donhauser, Z. J.; Mantooth, B. A.; Kelly, K. F.; Bumm, L. A.; Monnell, J. D.; Stapleton, J. J.; Price, D. W.; Rawlett, A. M.; Allara, D. L.; Tour, J. M.; Weiss, P. S. *Science* **2001**, *292*, 2303.
(12) Lewis, P. A.; Donhauser, Z. J.; Mantooth, B. A.; Smith, R. K.; Bumm, L. A.; Kelly, K. F.; Weiss, P. S. *Nanotechnology* **2001**, *12*, 231.
(13) Moore, A. M.; Mantooth, B. A.; Donhauser, Z. J.; Yao, Y. X.; Tour, J. M.; Weiss, P. S. *J. Am. Chem. Soc.* **2007**, *129*, 10352.
(14) Bumm, L. A.; Arnold, J. J.; Charles, L. F.; Dunbar, T. D.; Allara, D. L.; Weiss, P. S. *J. Am. Chem. Soc.* **1999**, *121*, 8017.
(15) Saavedra, H. M.; Thompson, C. M.; Hohman, J. N.; Crespi, V. H.; Weiss, P. S. *J. Am. Chem. Soc.* **2009**, *131*, 2252.
(16) Lewis, P. A.; Smith, R. K.; Kelly, K. F.; Bumm, L. A.; Reed, S. M.; Clegg, R. S.; Gunderson, J. D.; Hutchison, J. E.; Weiss, P. S. *J. Phys. Chem. B* **2001**, *105*, 10630.
(17) Smith, R. K.; Reed, S. M.; Lewis, P. A.; Monnell, J. D.; Clegg, R. S.; Kelly, K. F.; Bumm, L. A.; Hutchison, J. E.; Weiss, P. S. *J. Phys. Chem. B* **2001**, *105*, 1119.
(18) Schleyer, P. V.; Donaldson, M. M. *J. Am. Chem. Soc.* **1960**, *82*, 4645.
(19) Fujii, S.; Akiba, U.; Fujihira, M. *J. Am. Chem. Soc.* **2002**, *124*, 13629.
(20) Kitagawa, T.; Idomoto, Y.; Matsubara, H.; Hobara, D.; Kakiuchi, T.; Okazaki, T.; Komatsu, K. *J. Org. Chem.* **2006**, *71*, 1362.
(21) Katano, S.; Kim, Y.; Matsubara, H.; Kitagawa, T.; Kawai, M. *J. Am. Chem. Soc.* **2007**, *129*, 2511.
(22) Yang, W. L.; Fabbri, J. D.; Willey, T. M.; Lee, J. R. I.; Dahl, J. E.; Carlson, R. M. K.; Schreiner, P. R.; Fokin, A. A.; Tkachenko, B. A.; Fokina, N. A.; Meevasana, W.; Mannella, N.; Tanaka, K.; Zhou, X. J.; van Buuren, T.; Kelly, M. A.; Hussain, Z.; Melosh, N. A.; Shen, Z. X. *Science* **2007**, *316*, 1460.
(23) Willey, T. M.; Fabbri, J. D.; Lee, J. R. I.; Schreiner, P. R.; Fokin, A. A.; Tkachenko, B. A.; Fokina, N. A.; Dahl, J. E. P.; Carlson, R. M. K.; Vance, A. L.; Yang, W. L.; Terminello, L. J.; van Buuren, T.; Melosh, N. A. *J. Am. Chem. Soc.* **2008**, *130*, 10536.
(24) Clay, W. A.; Liu, Z.; Yang, W.; Fabbri, J. D.; Dahl, J. E.; Carlson, R. M. K.; Sun, Y.; Schreiner, P. R.; Fokin, A. A.; Tkachenko, B. A.; Fokina, N. A.; Pianetta, P. A.; Melosh, N.; Shen, Z.-X. *Nano Lett.* **2009**, *9*, 57.
(25) Dameron, A. A.; Charles, L. F.; Weiss, P. S. *J. Am. Chem. Soc.* **2005**, *127*, 8697.
(26) Dameron, A. A.; Hampton, J. R.; Smith, R. K.; Mullen, T. J.; Gillmor, S. D.; Weiss, P. S. *Nano Lett.* **2005**, *5*, 1834.
(27) Dameron, A. A.; Hampton, J. R.; Gillmor, S. D.; Hohman, J. N.; Weiss, P. S. *J. Vac. Sci. Technol. B* **2005**, *23*, 2929.
(28) Mullen, T. J.; Dameron, A. A.; Andrews, A. M.; Weiss, P. S. *Aldrichim. Acta* **2007**, *40*, 21.
(29) Srinivasan, C.; Mullen, T. J.; Hohman, J. N.; Anderson, M. E.; Dameron, A. A.; Andrews, A. M.; Dickey, E. C.; Horn, M. W.; Weiss, P. S. *ACS Nano* **2007**, *1*, 191.
(30) Dameron, A. A.; Mullen, T. J.; Hengstebeck, R. W.; Saavedra, H. M.; Weiss, P. S. *J. Phys. Chem. C* **2007**, *111*, 6747.
(31) Saavedra, H. M.; Barbu, C. M.; Dameron, A. A.; Mullen, T. J.; Crespi, V. H.; Weiss, P. S. *J. Am. Chem. Soc.* **2007**, *129*, 10741.
(32) Mullen, T. J.; Dameron, A. A.; Saavedra, H. M.; Williams, M. E.; Weiss, P. S. *J. Phys. Chem. C* **2007**, *111*, 6740.
(33) Laibinis, P. E.; Nuzzo, R. G.; Whitesides, G. M. *J. Phys. Chem.* **1992**, *96*, 5097.
(34) Zheng, T. C.; Burkart, M.; Richardson, D. E. *Tetrahedron Lett.* **1999**, *40*, 603.
(35) Greidanu, J. W.; Schwalm, W. J. *Can. J. Chem.* **1969**, *47*, 3715.
(36) Farcasiu, D.; Ghenciu, A.; Li, J. Q. *J. Catal.* **1996**, *158*, 116.
(37) Tanner, D. D.; Brownlee, B. G. *Can. J. Chem.* **1973**, *51*, 3366.
(38) Wilson, S. R.; Georgiadis, G. M.; Khatri, H. N.; Bartmess, J. E. *J. Am. Chem. Soc.* **1980**, *102*, 3577.
(39) Greidanu, J. W. *Can. J. Chem.* **1970**, *48*, 3593.
(40) Besocke, K. *Surf. Sci.* **1987**, *181*, 145.
(41) Frohn, J.; Wolf, J. F.; Besocke, K.; Teske, M. *Rev. Sci. Instrum.* **1989**, *60*, 1200.
(42) Moulder, J. F. *Handbook of X-ray Photoelectron Spectroscopy: A Reference Book of Standard Spectra for Identification and Interpretation of XPS Data*; Perkin-Elmer Corporation, Physical Electronics Division: Eden Prairie, Mn, 1992.
(43) Fairley, N. CasaXPS, 2005.
(44) Mullen, T. J. Nanoscale Self-and Directed Assemblies. Ph.D. Thesis, The Pennsylvania State University, University Park, PA, 2008.
(45) Mullen, T. J.; Dameron, A. A.; Weiss, P. S. *J. Phys. Chem. B* **2006**, *110*, 14410.
(46) Bard, A. J.; Faulkner, L. R. *Electrochemical Methods: Fundamentals and Applications*, 2nd ed.; John Wiley and Sons, Inc.: New York, 2001.
(47) Collard, D. M.; Fox, M. A. *Langmuir* **1991**, *7*, 1192.
(48) Noh, J.; Araki, T.; Nakajima, K.; Hara, M. *Mol. Cryst. Liq. Cryst.* **2001**, *371*, 95.
(49) Willey, T. M.; Vance, A. L.; van Buuren, T.; Bostedt, C.; Terminello, L. J.; Fadley, C. S. *Surf. Sci.* **2005**, *576*, 188.
(50) Schonenberger, C.; Jorritsma, J.; Sondaghuethorst, J. A. M.; Fokkink, L. G. J. *J. Phys. Chem.* **1995**, *99*, 3259.
(51) Delamarche, E.; Michel, B.; Kang, H.; Gerber, C. *Langmuir* **1994**, *10*, 4103.
(52) Bucher, J. P.; Santesson, L.; Kern, K. *Langmuir* **1994**, *10*, 979.
(53) Camillone, N.; Eisenberger, P.; Leung, T. Y. B.; Schwartz, P.; Scoles, G.; Poirier, G. E.; Tarlov, M. J. *J. Chem. Phys.* **1994**, *101*, 11031.
(54) Yamada, R.; Wano, H.; Uosaki, K. *Langmuir* **2000**, *16*, 5523.
(55) Poirier, G. E. *Langmuir* **1997**, *13*, 2019.
(56) Delamarche, E.; Michel, B.; Gerber, C.; Anselmetti, D.; Guntherodt, H. J.; Wolf, H.; Ringsdorf, H. *Langmuir* **1994**, *10*, 2869.
(57) Zhang, L. Z.; Goddard, W. A.; Jiang, S. Y. *J. Chem. Phys.* **2002**, *117*, 7342.
(58) Nowacki, W. *Helv. Chim. Acta* **1945**, *28*, 1233.
(59) Lussem, B.; Muller-Meskamp, L.; Karthauser, S.; Waser, R. *Langmuir* **2005**, *21*, 5256.
(60) Mullen, T. J.; Srinivasan, C.; Hohman, J. N.; Gillmor, S. D.; Shuster, M. J.; Horn, M. W.; Andrews, A. M.; Weiss, P. S. *Appl. Phys. Lett.* **2007**, *90*, 063114.
(61) Stranick, S. J.; Parikh, A. N.; Tao, Y. T.; Allara, D. L.; Weiss, P. S. *J. Phys. Chem.* **1994**, *98*, 7636.
(62) Bumm, L. A.; Arnold, J. J.; Dunbar, T. D.; Allara, D. L.; Weiss, P. S. *J. Phys. Chem. B* **1999**, *103*, 8122.
(63) Monnell, J. D.; Stapleton, J. J.; Jackiw, J. J.; Dunbar, T.; Reinerth, W. A.; Dirk, S. M.; Tour, J. M.; Allara, D. L.; Weiss, P. S. *J. Phys. Chem. B* **2004**, *108*, 9834.
(64) Monnell, J. D.; Stapleton, J. J.; Dirk, S. M.; Reinerth, W. A.; Tour, J. M.; Allara, D. L.; Weiss, P. S. *J. Phys. Chem. B* **2005**, *109*, 20343.
(65) Poirier, G. E. *Langmuir* **1999**, *15*, 1167.
(66) Poirier, G. E.; Fitts, W. P.; White, J. M. *Langmuir* **2001**, *17*, 1176.
(67) Fitts, W. P.; White, J. M.; Poirier, G. E. *Langmuir* **2002**, *18*, 1561.
(68) Fitts, W. P.; White, J. M.; Poirier, G. E. *Langmuir* **2002**, *18*, 2096.
(69) Schlenoff, J. B.; Li, M.; Ly, H. *J. Am. Chem. Soc.* **1995**, *117*, 12528.
(70) Kolega, R. R.; Schlenoff, J. B. *Langmuir* **1998**, *14*, 5469.
(71) Shon, Y. S.; Lee, T. R. *J. Phys. Chem. B* **2000**, *104*, 8192.
(72) Balss, K. M.; Coleman, B. D.; Lansford, C. H.; Haasch, R. T.; Bohn, P. W. *J. Phys. Chem. B* **2001**, *105*, 8970.
(73) Imabayashi, S.; Hobara, D.; Kakiuchi, T.; Knoll, W. *Langmuir* **1997**, *13*, 4502.
(74) Kakiuchi, T.; Usui, H.; Hobara, D.; Yamamoto, M. *Langmuir* **2002**, *18*, 5231.
(75) Walczak, M. M.; Popenoe, D. D.; Deinhammer, R. S.; Lamp, B. D.; Chung, C. K.; Porter, M. D. *Langmuir* **1991**, *7*, 2687.
(76) Hobara, D.; Miyake, O.; Imabayashi, S.; Niki, K.; Kakiuchi, T. *Langmuir* **1998**, *14*, 3590.
(77) Hobara, D.; Ota, M.; Imabayashi, S.; Niki, K.; Kakiuchi, T. *J. Electroanal. Chem.* **1998**, *444*, 113.
(78) Widrig, C. A.; Chung, C.; Porter, M. D. *J. Electroanal. Chem.* **1991**, *310*, 335.
(79) Porter, M. D.; Bright, T. B.; Allara, D. L.; Chidsey, C. E. D. *J. Am. Chem. Soc.* **1987**, *109*, 3559.
(80) Calvente, J. J.; Kovacova, Z.; Andreu, R.; Fawcett, W. R. *J. Chem. Soc., Faraday Trans. 1* **1996**, *92*, 3701.
(81) Calvente, J. J.; Kovacova, Z.; Sanchez, M. D.; Andreu, R.; Fawcett, W. R. *Langmuir* **1996**, *12*, 5696.
(82) Laibinis, P. E.; Bain, C. D.; Whitesides, G. M. *J. Phys. Chem.* **1991**, *95*, 7017.
(83) Nuzzo, R. G.; Dubois, L. H.; Allara, D. L. *J. Am. Chem. Soc.* **1990**, *112*, 558.
(84) Klünder, K. Photoelectron Spectroscopy on Molecular Diamond. Diploma Thesis, Technical University of Berlin, 2007.
(85) Snis, A.; Matar, S. F. *Phys. Rev. B* **1999**, *60*, 10855.
(86) Cabarcos, O. M.; Shaporenko, A.; Weidner, T.; Uppili, S.; Dake, L. S.; Zharnikov, M.; Allara, D. L. *J. Phys. Chem. C* **2008**, *112*, 10842.
(87) Bistričić, L.; Baranović, G.; Mlinarić-Majerski, K. *Spectrochim. Acta, Part A* **1995**, *51*, 1643.
(88) Jensen, J. O. *Spectrochim. Acta, Part A* **2004**, *60*, 1895.
(89) Fox, J. J.; Martin, A. E. *Proc. R. Soc. London, A* **1940**, *175*, 208.
(90) Mullen, T. J.; Srinivasan, C.; Shuster, M. J.; Horn, M. W.; Andrews, A. M.; Weiss, P. S. *J. Nanopart. Res.* **2008**, *10*, 1231.
(91) Kang, H.; Lee, H.; Kang, Y.; Hara, M.; Noh, J. *Chem. Commun.* **2008**, 5197.
(92) Kwon, S.; Choi, Y.; Choi, J.; Kang, H.; Chung, H.; Noh, J. *Ultramicroscopy* **2008**, 1311.

JP810048N